Strong Induced-Dipole-Field Oscillations of the $dt\mu$ System above the $t\mu(n = 2)$ Threshold

Ken-ichi Hino[1] and Joseph H. Macek[1,2]
[1]*Department of Applied Physics and Chemistry, University of Electro-Communications, Chofu, Tokyo 182, Japan and Atomic Physics Laboratory, The Institute of Physical and Chemical Research (RIKEN), Wako, Saitama 351-01, Japan*
[2]*Department of Physics and Astronomy, University of Tennessee, Knoxville, Tennessee 37996 and Oak Ridge National Laboratory, Oak Ridge, Tennessee 37831*
(Received 20 February 1996)

Elastic, inelastic, and muon transfer processes of the $dt\mu$ system above the $t\mu(n = 2)$ threshold are studied theoretically using the hyperspherical coordinate method. Strong oscillation structures in the cross sections for these processes due to strong, attractive dipole potentials in this system are found. In addition to the expected Gailitis-Damburg Stark mixing oscillations, unexpected oscillations due to diabatic couplings of channels lacking attractive dipole potentials with those that have them are evident. The two types of oscillations interfere to produce the structure that appears in the computed cross sections. [S0031-9007(96)01715-2]

PACS numbers: 36.10.Dr, 31.15.Ja

Investigations of elementary atomic processes for a $dt\mu$ molecule are important for disentangling complicated phenomena underlying muon catalyzed fusion (μCF) and, further, to understand the general Coulomb three-body problem beyond the validity of the infinite nuclear mass approximation conventionally applied to diatomic molecules and two-electron atoms [1]. Recently, of particular interest in μCF are muon transfers in the $n \geq 2$ manifolds and Feshbach resonances thought to play decisive roles for realizing a high formation rate of the resonant complex $[(dt\mu)^* dee]$ below the $t\mu(n = 2)$ threshold [2]. Both processes may be important in resolving a long-standing puzzle of discrepancy that the experimentally measured muon cycling rate is smaller than that predicted by theory [3]. Such atomic processes relevant to excited $dt\mu$ molecules are influenced by a long-range attractive dipole interaction $-\alpha/(2MR^2)$, where α is associated with a dipole moment of degenerate states of $t\mu$ ($d\mu$) atoms induced by collision partners d (t) at a distance R with the reduced mass M. The dipole interaction produces an infinite number of bound or resonance states below threshold, and oscillations of cross sections with energy above threshold. The latter effect is called the Gailitis-Damburg (GD) oscillation [4]. Exploration of this threshold behavior in the electron-hydrogen collision has proved difficult due to its negligibly weak influences upon the overall cross sections [5,6]. To our knowledge, there is no report on this effect in extremely low-energy ion-atom collisions. Strong dipole interactions of electrons with permanent dipole moments produce analogous effects in electron scattering by polar molecules [7].

Strong GD oscillations are expected in $dt\mu$. The magnitudes of α are 66.25 and 68.70 [in the muon atomic unit (m.a.u.)] for the respective fragments of d-$t\mu(n = 2)$ and t-$d\mu(n = 2)$ with total angular momentum $J = 0$. These values are more than ten times greater than the corresponding ones, of the order of 5.08 (in the usual atomic unit) for the electron-hydrogen system. Such large magnitudes of α in $dt\mu$ are related to its large reduced mass M of about 10 (m.a.u.) [8]. In this Letter, we investigate the effect of oscillations in this system. Such oscillations for $dt\mu$ molecules have not been studied previously. Our calculations are limited to only $J = 0$, where the GD oscillations are strongest. The GD oscillations are present for values of J up to $J = 7$ in the $n = 2$ manifolds with their frequency gradually deceasing with increasing J. We defer calculations for higher J to a subsequent paper [9]. Moreover, Lamb shift splittings (about 0.2 eV) of the $2s$ and $2p$ states are not considered. The muon atomic unit is used throughout unless otherwise stated. The physical values adopted here for masses and the Rydberg constant were taken from [10].

We employ the hyperspherical coordinate method to analyze the Coulomb three-body system of $dt\mu$ since it treats all three particles on equal footing, irrespective of mass and charge ratios [11]. This method also guarantees exact dissociation energies of $d\mu$ and $t\mu$ fragments. Hyperspherical adiabatic potential curves and channel functions are first computed and used to set up hyperspherical close coupling equations. The hyperspherical multichannel equations with suitable scattering boundary conditions are solved, and the scattering matrix is extracted.

The adiabatic potential curves are obtained by expanding channel wave functions in hydrogenic basis sets situated around both nuclei of d and t. Thirty hydrogenic bases up to the $n = 5$ states are incorporated [12]. In addition to these, fifteen hyperspherical harmonics are included to improve numerical convergences in the small hyperradius (ρ) region. The nonorthogonal basis set is transformed to an orthogonal basis set by prediagonalizing its overlap matrix and eliminating the ill-behaved eigenvectors whose eigenvalues are negative or positive and very small.

Evaluating integrals for different-center matrix elements is the most critical step in our calculation. It is the

 0031-9007/96/77(21)/4310(4)$10.00

main cause of numerical inaccuracies and the most time-consuming step because of the cumbersome presence of the Coulomb singularities in the two-dimensional plane. Here we have to evaluate the matrix elements of different-center hydrogenic bases. For this purpose, the Laguerre polynomials in the hydrogenic basis of either center are expanded in terms of the Gaussian basis set with high accuracy. The Gaussian functions are amenable to direct transformation from one coordinate system into the other [9]. As a result, all different-center matrix elements are reduced to one-dimensional integrals over a single hyperangle, and the locus of Coulomb singularities in the two-dimensional plane is transformed to just points in this coordinate.

In Fig. 1 we show four of the calculated potential curves converging to the $n = 2$ manifolds. We label these potentials as $t\mu(+)$, $t\mu(-)$, $d\mu(+)$, and $d\mu(-)$ in the order of increasing energy in the diabatic sense. In the small ρ region ($\rho \leq 100$), the obtained accuracy is to about five figures. In the large ρ region ($\rho \geq 300$), high accuracy is indispensable since, as seen later, we deal with the extremely low-energy collisions at 0.001 eV (1.778×10^{-7} m.a.u.). The high accuracy to ten figures was reached since the eigenfunctions are well approximated by the well-behaved hydrogenic basis functions in the asymptotic region.

Expanding the total wave function Ψ in terms of

$$\Psi_\nu(\rho, \Omega) = \sum_\mu \Phi_\mu(\rho, \Omega) F_{\mu\nu}(\rho), \qquad (1)$$

where $\Phi_\mu(\rho, \Omega)$ is a channel wave function with Ω being all angular variables, yields the adiabatic expression for the hyperspherical multichannel equation for $\mathbf{F}$:

$$\mathbf{F}'' + 2\mathbf{P}\mathbf{F}' + \left[\frac{1}{4\rho^2} + 2(E - \mathbf{U}) + \mathbf{W}\right]\mathbf{F} = 0. \qquad (2)$$

Here the matrix notations are used. $\mathbf{P}$ and $\mathbf{W}$ are derivative coupling matrices defined by $\langle \mathbf{\Phi} \,|\, \mathbf{\Phi}' \rangle$ and $\langle \mathbf{\Phi} \,|\, \mathbf{\Phi}'' \rangle$, respectively. $\mathbf{U}$ is the adiabatic potential matrix mentioned above.

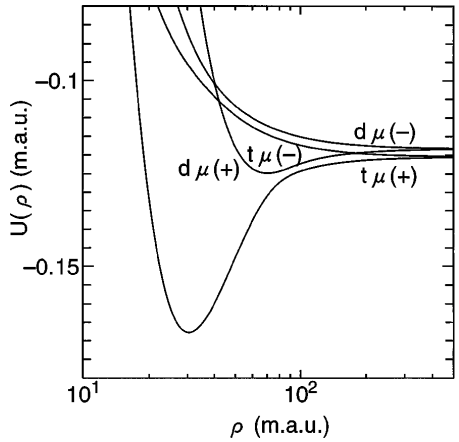

FIG. 1. Hyperspherical adiabatic potentials $U(\rho)$ (m.a.u.) converging to the $n = 2$ dissociation limits for $J = 0$ versus hyperradius ρ (m.a.u.).

We first divide the ρ interval into a number of small sectors and inspect whether or not there exist strong avoided crossings within each sector. If so, the adiabatic expression of Eq. (2) is not suitable as it is. In this case, $\mathbf{P}$ is partitioned as $\mathbf{P} = \mathbf{P}_0 + \mathbf{P}_x$, where $\mathbf{P}_x$ has nonzero elements pertaining to the avoided crossings, and the remainder $\mathbf{P}_0$ is a smooth function of ρ. The partial diabatic transformation $\mathbf{F} = \mathbf{A}\tilde{\mathbf{F}}$ is done to remove sharp spike couplings of $\mathbf{P}_x$ [13]. The unitary matrix $\mathbf{A}$ is obtained by solving $\mathbf{A}' = -\mathbf{P}_x\mathbf{A}$ within the sector. Multichannel equations for $\tilde{\mathbf{F}}$ are obtained using this transformation. They are similar to Eq. (2). $\mathbf{P}$, $\mathbf{W}$, and $\mathbf{U}$ are replaced by the respective tilded quantities: $\tilde{\mathbf{P}} = \mathbf{A}^{-1}\mathbf{P}_0\mathbf{A}$, $\tilde{\mathbf{W}} = \mathbf{A}^{-1}[\mathbf{W} - (\mathbf{P}_x' + \mathbf{P}_x^2) - 2\mathbf{P}_0\mathbf{P}_x]\mathbf{A}$, and $\tilde{\mathbf{U}} = \mathbf{A}^{-1}\mathbf{U}\mathbf{A}$. $\tilde{\mathbf{W}}$ is a smooth function of ρ since sharp couplings in $\mathbf{W}$ are cancelled by $\mathbf{P}_x' + \mathbf{P}_x^2$.

The S matrix $\mathbf{S}'$ in the dipole representation, i.e., the representation that diagonalizes the long-range dipole interaction, is obtained using the matching procedure of Christensen-Dalsgaard [14] with free-field wave functions for the $n = 1$ manifolds and dipole-field ones for the $n \geq 2$ manifolds [15]. This matrix is furthermore transformed into the S matrix $\mathbf{S}$ in the usual angular momentum representation by

$$\mathbf{S} = \mathbf{V}^{(+)}\mathbf{S}'\mathbf{V}^{(-)\dagger}, \qquad (3)$$

where the transformation matrices $\mathbf{V}^{(\pm)}$ are unitary [4].

The twenty-channel coupled equations were solved with the matching radius chosen to be 20 000 m.a.u. This calculation includes channels up to the $n = 4$ manifolds. Such a large distance is required to impose dipole-field boundary conditions safely upon the radial wave function $\mathbf{F}$ even at the lowest energy of 0.001 eV. The convergence of the present calculations was confirmed by comparison with corresponding twelve- and six-channel calculations, which include channels up to the $n = 3$ and $n = 2$ manifolds, respectively. The six-channel calculations reproduce the results by the twenty-channel ones fairly well.

The squared magnitudes of the transition matrix elements in the dipole representation $|T'_{f'i'}|^2$ for the elastic and inelastic processes within the $t\mu(n = 2)$ manifold and for the muon transfer processes from the $d\mu(n = 2)$ to the $t\mu(n = 2)$ manifold are shown in Figs. 2 and 3. As seen in Fig. 2, the series of the Feshbach resonances converging to the $d\mu(n = 2)$ dissociation limit are found at 8.24, 10.29, 11.21, and 11.63 eV.

Strong oscillations are observed in every process above their respective thresholds. To examine the origin of the oscillation structures, notice that the asymptotic wave function $F_{\mu\mu}$ for the attractive dipole channel μ incorporates the known phase $\phi_\mu(k_\mu, \beta_\mu)$ dependent on the argument $\beta_\mu \ln(k_\mu/2)$, with β_μ and k_μ associated with the strength of the potential and momentum of the dissociated fragment [15]. In the lower-energy region, where the

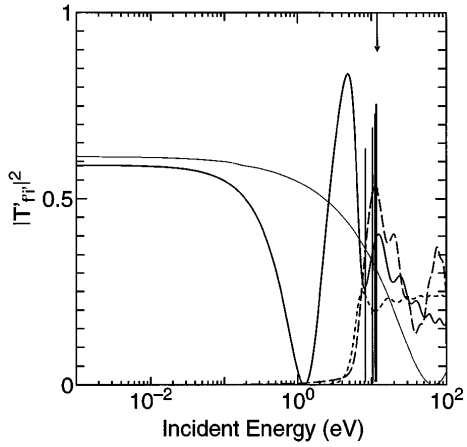

FIG. 2. $|T'_{f',i'}|^2$ versus the incident energy (eV) in the center-of-mass frame measured from the $t\mu(n = 2)$ threshold. The solid, the long-dashed, and the short-dashed lines are the twenty-channel calculations for $|T'_{t\mu(+),t\mu(+)}|^2$, $|T'_{t\mu(-),t\mu(-)}|^2$, and $|T'_{t\mu(-),t\mu(+)}|^2$, respectively. The thin solid line is the six-channel pilot calculation for $|T'_{t\mu(+),t\mu(+)}|^2$. Here, $|T'_{t\mu(+),t\mu(-)}|^2$ is equal to $|T'_{t\mu(-),t\mu(+)}|^2$. The arrow at 12.01 eV indicates the dissociation limit of $d\mu(n = 2)$. The vertical lines just below this are a series of the Feshbach resonances (see text).

couplings with other channels are still negligibly small, the phase shift $\delta_\mu(k_\mu)$ exhibits the weak energy dependence in the present dipole representation. The couplings become more dominant with increasing incident energy. Specifically, the coupling with other attractive dipole channels, say, ν, would cause a noticeable oscillating energy dependence of the phase shift $\delta_\mu(k_\mu)$ in the μth channel through $\phi_\nu(k_\nu, \beta_\nu)$. Similar energy dependences would also appear in phase shifts pertinent to repulsive dipole channels via a combination of couplings with nearby attractive dipole channels.

To confirm this speculation we implemented six-channel pilot calculations by turning off all nonadiabatic couplings in **P** and **W** between the upper channels $d\mu(\pm)$ and the lower ones $t\mu(\pm)$ but retaining the Landau-Zener type crossing between $d\mu(+)$ and $t\mu(-)$ in the vicinity of $\rho = 179.50$. Without this crossing little muon transfers from the upper to the lower channels takes place. This result seen in Fig. 2 shows no oscillation in energy for the elastic process $t\mu(+) \rightarrow t\mu(+)$. In Fig. 3, the result of the pilot calculation for the transfer process $d\mu(+) \rightarrow t\mu(-)$ is shown. The oscillations seen above $\sim$5 eV are thought to be due to oscillation via $\phi_\mu(k_\mu, \beta_\mu)$ of the $d\mu(+)$ channel since there are no couplings of the upper channels with the lower attractive channel $t\mu(+)$.

Figures 4 and 5 show the squares of the transition matrix elements $|T_{fi}|^2$ in the usual representation. The conspicuous GD oscillations result from the strong Stark mixing between $2s$ and $2p$ states of the same manifold through the transformation of Eq. (3). Irregular oscillation patterns arising above $\sim$5–10 eV are thought to be due to the interferences of the Stark mixing components with components attributed to the above-mentioned diabatic coupling mechanism.

Finally, we examine whether or not the rate constant λ still shows these oscillations. The Stark mixing process $d + t\mu(2s) \rightarrow d + t\mu(2p)$ is considered as an illustration. The discussion below would also hold correctly in other processes. $|T_{t\mu(2p),t\mu(2s)}|^2$ in Fig. 4 is well expressed as the closed analytic form $\frac{1}{4}\sin^2(\frac{\beta}{2}\ln\frac{\epsilon}{\epsilon_0})$. This is obtained by using the two-channel approximation of $\mathbf{S}'$ including only $t\mu(\pm)$ channels. Here ϵ is the incident

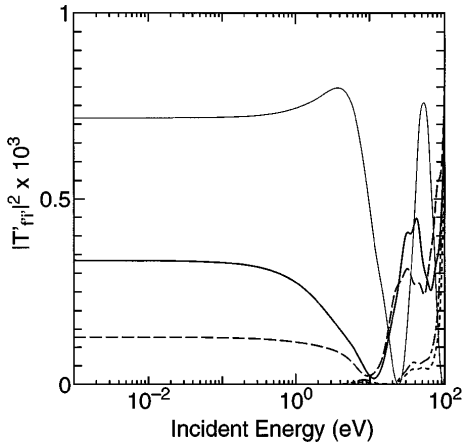

FIG. 3. $|T'_{f',i'}|^2$ versus the incident energy (eV) in the center-of-mass frame measured from the $d\mu(n = 2)$ threshold. The solid, the long-dashed, the short-dashed, and the chain lines are the twenty-channel calculations for $|T'_{t\mu(-),d\mu(+)}|^2$, $|T'_{t\mu(+),d\mu(+)}|^2$, $|T'_{t\mu(+),d\mu(-)}|^2$, and $|T'_{t\mu(-),d\mu(-)}|^2$, respectively. The thin solid line is the six-channel pilot calculation for $|T'_{t\mu(-),d\mu(+)}|^2$.

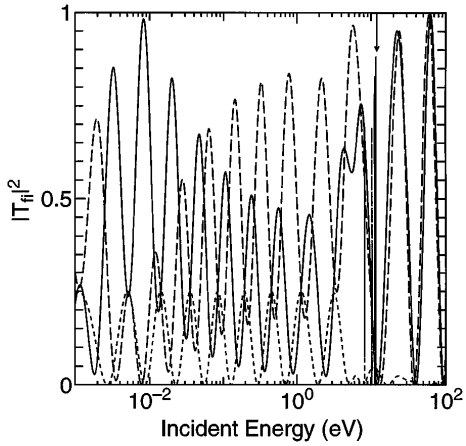

FIG. 4. $|T_{f,i}|^2$ versus the incident energy (eV) in the center-of-mass frame measured from the $t\mu(n = 2)$ threshold. The solid, the long-dashed, and the short-dashed lines are the twenty-channel calculations for $|T_{t\mu(2s),t\mu(2s)}|^2$, $|T_{t\mu(2p),t\mu(2p)}|^2$, and $|T_{t\mu(2p),t\mu(2s)}|^2$, respectively. Here, $|T_{t\mu(2s),t\mu(2p)}|^2$ is equal to $|T_{t\mu(2p),t\mu(2s)}|^2$.

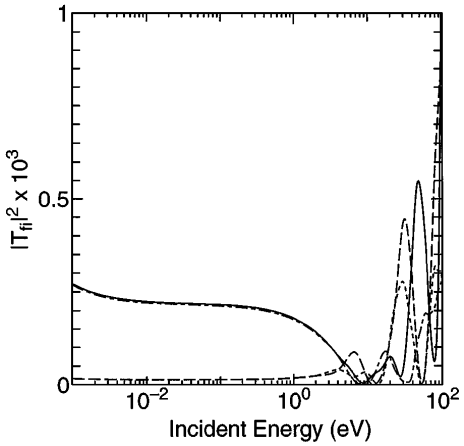

FIG. 5. $|T_{f,i}|^2$ versus the incident energy (eV) in the center-of-mass frame measured from the $d\mu(n = 2)$ threshold. The solid, the long-dashed, the short-dashed, and the chain lines are the twenty-channel calculations for $|T_{t\mu(2p),d\mu(2s)}|^2$, $|T_{t\mu(2s),d\mu(2s)}|^2$, $|T_{t\mu(2s),d\mu(2p)}|^2$, and $|T_{t\mu(2p),d\mu(2p)}|^2$, respectively.

energy in the center-of-mass frame, and $\beta = \sqrt{\alpha^2 - 1/4}$. ϵ_0 is a weakly energy-dependent parameter upon the S matrix elements of $\mathbf{S}'$. For the sake of simplicity, this parameter is regarded as constant. Averaging the associated cross section over the Maxwellian velocity distribution yields the approximate expression of λ besides an unimportant multiplicative constant as $\lambda \sim \tau^{-1/2}[1 - c(\pi\beta)\cos(\beta \ln \frac{\tau}{\epsilon_0})]$, where τ is temperature multiplied by the Boltzmann constant and $c(x) = \sqrt{x/\sinh x}$. Exact values of λ obtained by direct numerical integration of the calculated cross section shown in Fig. 4 can be well reproduced up to τ of about a few eV by this simple expression.

According to this analytic form, the appearance of the oscillations with respect to τ is suppressed by a negligibly small value of the factor $c(\pi\beta)$ in the present case, where $\beta = 8.12$ ($\alpha = 66.25$). The fine structures of rapid oscillations in the cross section resulting from a large β are completely smoothed out in the associated rate constant by the Maxwellian average. However, it is expected that more coarse structures of oscillations due to a smaller β would remain in the rate constant. Such a smaller value of β would be realized in the contribution of higher partial waves of J in the present process since larger centrifugal barriers reduce the magnitude of the attractive dipole potential to some extent. This simple model shows that, for β smaller than about 2, λ begins to exhibit oscillations.

We conclude that the strong dipole fields induced in $dt\mu$ systems yield noticeable oscillation structures in $\mathbf{T}'$ due to the diabatic couplings with attractive dipole channels. These oscillations would be retained even in the nondegenerate system, such as a more realistic system incorporating Lamb shift splittings, since the effect originates from the presence of the attractive dipole potentials in the outer region of ρ roughly from 100 to 1000 m.a.u., where the Lamb shift is small compared with the channel potentials. In such a nondegenerate $dt\mu$ system, however, the GD oscillations in $\mathbf{T}$ owing to the Stark mixing would be absent for energies between 0 and about 0.2 eV. These oscillations appear in the higher energy region in an irregular way due to interferences with oscillations connected with diabatic couplings. They are also present for values of higher J up to $J = 7$ in the $n = 2$ manifolds. Additionally, for such higher values of J, oscillations may be present in the corresponding rate constants as well.

K. H. gratefully acknowledges extensive discussion with A. Igarashi, I. Shimamura, and S. Watanabe throughout this work. This research is supported by Grant-in-Aid for Encouragement of Young Scientists from the Ministry of Education, Science and Culture of Japan, and by the National Science Foundation under Grant No. PHY-9222489. K. H. thanks the Japanese Ministry of Education and the Japan Society for the Promotion of Science for supporting his stay in the U.S. The present numerical computations were also supported in part by the Institute of Physical and Chemical Research (RIKEN).

[1] L. I. Ponomarev, At. Phys. **10**, 197 (1986).
[2] P. Froelich and J. Wallenius, Phys. Rev. Lett. **75**, 2108 (1995).
[3] A. N. Anderson, in *Muon-Catalyzed Fusion*, edited by Steven E. Jones, Johann Rafelski, and Hendrik J. Monkhorst, AIP Conf. Proc. No. 181 (AIP, New York, 1988), p. 57.
[4] M. Gailitis and R. Damburg, Proc. Phys. Soc. **82**, 192 (1963).
[5] C.-R. Liu and A. F. Starace, Phys. Rev. Lett. **62**, 407 (1989).
[6] H. R. Sadeghpour, C. H. Greene, and M. Cavagnero, Phys. Rev. A **45**, 1587 (1992).
[7] D. W. Norcross and L. A. Collins, Adv. At. Mol. Phys. **18**, 341 (1982).
[8] I. Shimamura, Phys. Rev. A **40**, 4863 (1989).
[9] K. Hino and J. H. Macek (unpublished).
[10] E. R. Cohen and B. N. Taylor, CODATA Bull. **63** (1986) [J. Res. Natl. Bur. Stand. **92**, 85 (1987)].
[11] E. A. Soloviev and S. I. Vinitsky, J. Phys. B **18**, L557 (1985).
[12] C. D. Lin, Phys. Rev. A **23**, 1585 (1981).
[13] F. T. Smith, Phys. Rev. **179**, 111 (1969).
[14] B. L. Christensen-Dalsgaard, Phys. Rev. A **29**, 2242 (1984).
[15] C. H. Greene, U. Fano, and G. Strinati, Phys. Rev. A **19**, 1485 (1979).